JOURNAL OF SYNCHROTRON RADIATION
ISSN 1600-5775

X-ray natural circular dichroism in langasite crystal

Alexey P. Oreshko,[a]* Elena N. Ovchinnikova,[a] Andrei Rogalev,[b] Fabrice Wilhelm,[b] Boris V. Mill[a] and Vladimir E. Dmitrienko[c]

[a]Faculty of Physics, M. V. Lomonosov Moscow State University, Leninskie Gory, Moscow 119991, Russian Federation, [b]European Synchrotron Radiation Facility, 71 Avenue des Martyrs, CS 40220, Grenoble 38043, France, and [c]A. V. Shubnikov Institute of Crystallography, Federal Scientific Research Centre 'Crystallography and Photonics' of Russian Academy of Sciences, Leninskiy Prospekt 59, Moscow 119333, Russian Federation.
*Correspondence e-mail: ap.oreshko@physics.msu.ru

Received 21 June 2017
Accepted 23 October 2017

Edited by V. Favre-Nicolin, CEA and Université Joseph Fourier, France

Keywords: optical activity; circular dichroism; X-ray absorption spectra.

Optical activity in the X-ray range stems from the electric-dipole–electric-quadrupole interference terms mixing multipoles of opposite parity, and can be observed exclusively in systems with broken inversion symmetry. The gyration tensor formalism is used to describe the X-ray optical activity in langasite $La_3Ga_5SiO_{14}$ crystal with the *P*321 space group. An experimental study of the X-ray natural circular dichroism (XNCD) near the Ga *K*-edge in $La_3Ga_5SiO_{14}$ single crystal was performed at ESRF beamline ID12, both along and perpendicular to the crystal optical axis. The combination of the quantum mechanical calculations and high-quality experimental results has allowed us to separate the contributions into X-ray absorption and XNCD spectra of Ga atoms occupying three distinct Wyckoff positions.

1. Introduction

Since the discovery by Arago (Arago, 1811) and Biot (Biot, 1812) that crystalline quartz induces a rotation of the plane of polarization of visible light, the optical activity (OA) of single crystals has fascinated many successive generations of physicists. It was, however, only at the end of the 20th century that X-ray natural circular dichroism (XNCD) was detected in quite a few non-centrosymmetric crystals (Goulon *et al.*, 1998, 1999; Alagna *et al.*, 1998; Stewart *et al.*, 1999). Such experiments, which were performed about 100 years after the discovery of X-rays (Röntgen, 1898) and of circular dichroism in the visible spectral range (Cotton, 1895), became feasible due to the availability of intense beams of circularly polarized X-rays at third-generation synchrotron radiation sources. It has been known for many years (Nye, 1957; Landau & Lifshitz, 1960; Agranovich & Ginzburg, 1984; Yariv & Yeh, 1984) that OA in crystals is a tensor property resulting from the spatial dispersion of the dielectric response, *i.e.* the radiation–matter interactions depend on the space variable **r** and on the light wavevector **k**. OA refers to the first-order terms (linear in **k**) and is described by a rank-3 antisymmetric tensor, commonly referred to as the gyration tensor. The crystal symmetry imposes certain restrictions on the components of the gyration tensor (Jerphagnon & Chemla, 1976; Jerphagnon *et al.*, 1978). For example, all components of the gyration tensor are zero in centrosymmetric crystals. To summarize, out of the 21 non-centrosymmetric crystal classes (crystallographic point groups), 18 have a non-zero gyration tensor and are said to be optically active or gyrotropic. Note that among them only 11 crystal classes exhibit enantio-

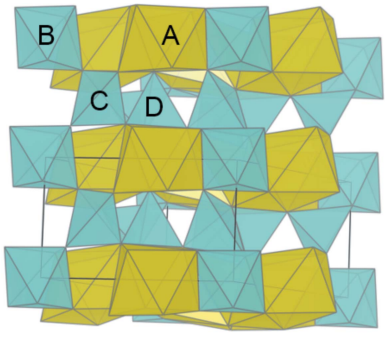

morphism and thus are chiral. It then becomes quite obvious that enantiomorphism (or chirality) and optical activity are two distinct concepts that should not be mixed together.

The decomposition of the Cartesian rank-3 gyration tensor into irreducible representations with respect to the operations of the group SO_3 was shown to yield (Jerphagnon & Chemla, 1976; Jerphagnon *et al.*, 1978) a pseudo-scalar, a polar vector and a traceless symmetric pseudo-tensor of rank-2, so-called pseudo-deviator. It has long been recognized that only chiral crystal classes have a non-zero pseudo-scalar part. On the other hand, gyrotropic crystals featuring a large pseudo-deviator part are most often showing a large non-linear susceptibility at visible wavelengths. More important for the present study is the link between the macroscopic gyration tensor and the microscopic susceptibility tensor: Buckingham & Dunn (1971) and Barron (1971, 1982) were the first to point out that the electric-dipole–electric-quadrupole ($E1.E2$) interference term contributed to the pseudo-deviator part of the gyration tensor but not to the pseudo-scalar which was identified with the electric-dipole–magnetic-dipole ($E1.M1$) mechanism.

In the visible spectral range, both the pseudo-scalar and the pseudo-deviator contribute to OA, whereas, in the X-ray range, the pseudo-deviator part only gives rise to natural circular dichroism (Goulon *et al.*, 1998, 1999). The reason for this is that the $E1.M1$ interference terms, which dominate OA measured with visible light, become vanishingly small in X-ray spectroscopy. The $E1.M1$ contribution implies a significant magnetic dipole transition probability and this is strongly forbidden in a non-relativistic approach due to the radial orthogonality of core with valence and continuum states involved in the X-ray absorption process. This restriction could be partially removed in fully relativistic formalism or due to relaxation of the core-hole. In contrast, electric quadrupolar ($E2$) transitions, which play only a marginal role at visible wavelengths, can become significant in the X-ray range since their magnitude increases with photon energy (Brouder, 1990). It is now well documented (see, for example, Goulon *et al.*, 2003*b*) that the interference electric-dipole–electric-quadrupole ($E1.E2$) terms are responsible for most OA-related effects observed in the X-ray range: natural circular dichroism (Goulon *et al.*, 1998; Alagna *et al.*, 1998), non-reciprocal linear dichroism (Goulon *et al.*, 2000; van der Laan, 2001), magnetochiral dichroism (Goulon *et al.*, 2002; Sessoli *et al.*, 2015) and the so-called Voigt-Fedorov dichroism observable in scattering experiments (Goulon *et al.*, 2007).

The electric-dipole–electric-quadrupole $E1.E2$ interference terms mix multipole transition moments of opposite parity, and this allows the mixed valence states to be probed by XNCD (Natoli *et al.*, 1998; Okutani *et al.*, 1999; Peacock & Stewart, 2001; Goulon *et al.*, 2003*a*,*b*). Moreover, XNCD makes it possible to determine the absolute configuration of chiral crystals (Rogalev *et al.*, 2008*a*; Sessoli *et al.*, 2015) similarly to natural circular dichroism or optical rotation in the visible region but with an element selectivity that is inherent to X-ray spectroscopy. This knowledge is especially important for systems, properties of which depend on their chirality, *e.g.* in bio- and pharmaceutical industry, in chiral liquid crystals, magnetoelectrics and other multifunctional materials.

The physical properties of a solid and its crystal structure are closely related and understanding this relationship is one of the greatest challenges of material science, especially in view of engineering new compounds. This is particularly true for multifunctional materials whose properties, like ferromagnetism or piezoelectricity, strongly depend on the symmetry of a substance. The langasite family of crystals, the archetype of which is $La_3Ga_5SiO_{14}$ (hence the name), form a formidable playground for designing multifunctional materials. These crystals were discovered in the 1980s in the former Soviet Union (Belokoneva & Belov, 1981; Mill *et al.*, 1982; Mill & Pisarevsky, 2000) and widely studied due to their piezoelectric and non-linear optical properties (Ohsato *et al.*, 2012; Chilla *et al.*, 2001; Roshchupkin *et al.*, 2003; Stade *et al.*, 2002) related to the non-centrosymmetric crystal structure. The langasite structure belongs to the trigonal non-centrosymmetric $P321$ space group. The general formula is $A_3BC_3D_2O_{14}$, which contains four different cationic sites. The decahedral A site and the octahedral B site form a layer at $z = 0$, whereas the two tetrahedral sites C and D are located on the plane $z = 1/2$ (see Fig. 1). Due to this atomic arrangement, the langasite structure is able to accommodate a large number of different cations with various sizes and valences, leading to a wide variety of isostructural compounds. Whenever one of the cations is substituted by magnetic ions, the crystals provide interesting examples of multiferroics with remarkable optical properties (Pikin & Lyubutin, 2012; Lee *et al.*, 2010) and even may lead to the appearance of exotic magnetic structure (Zorko *et al.*, 2011; Marty *et al.*, 2010; Scagnoli *et al.*, 2013; Ramakrishnan *et al.*, 2017). Many other physical properties of langasites can be tailored as well by properly choosing the substituted cations and their position in the structure (Takeda *et al.*, 2011; Sato *et al.*, 1998; Adachi *et al.*, 2003). That is why a detailed knowledge of the electronic properties corresponding to different crystallographic positions in langasites is very important.

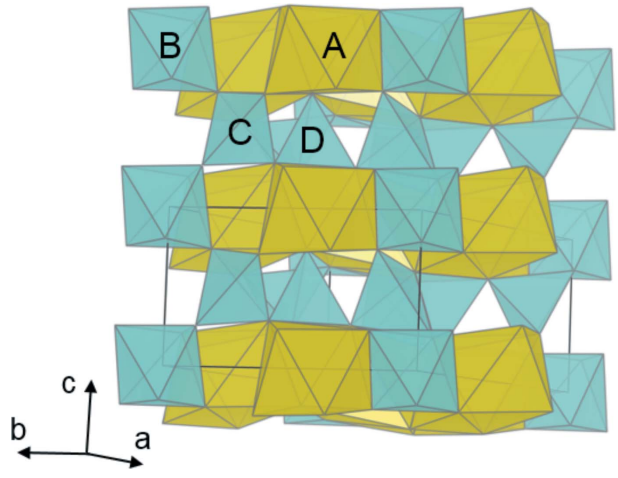

Figure 1
Crystal structure of $La_3Ga_5SiO_{14}$.

Here, we combined element-specific XNCD spectroscopy and *ab initio* quantum mechanical calculations to study local electronic properties of $La_3Ga_5SiO_{14}$ single crystal. As we mentioned earlier, XNCD is the most appropriate technique to study the hybridization of electronic states of opposite parity, which are at the origin of non-linear optical properties, and to give a useful insight into the electronic structure of the whole family of langasite compounds. Unfortunately, XNCD, as any X-ray absorption-based technique, measures the signal at the absorption edge of a given chemical element averaged over all crystallographic positions which it occupies in the crystal. Thus, X-ray dichroism is an element-specific and edge-selective technique, but not site-selective (Brouder *et al.*, 2008). To overcome this difficulty, one can exploit resonant X-ray diffraction which is an element-specific and site-selective method due to the phase shift between the waves scattered by different atomic sites (Hodeau *et al.*, 2001; Dmitrienko *et al.*, 2005). However, the symmetry of the langasite crystals does not impose any reflection conditions and all resonant atoms occupying non-equivalent crystallographic sites simultaneously contribute to the allowed reflections measured in X-ray diffraction experiments. Being more time-consuming, the resonant diffraction methods have no advantages in studying the electronic structure of langasites and rely on numerical simulations that are no less complicated than those used for the XNCD.

The present paper starts with a detailed analysis of the relation between the microscopic and macroscopic description of X-ray optical activity in crystals with *P*321 symmetry, especially the langasite family of crystals. We show that analysis of the Ga *K*-edge XNCD in $La_3Ga_5SiO_{14}$ single crystal based on quantum mechanical calculations allows one to disentangle the contributions from crystallographically different atomic sites.

2. X-ray optical activity

Recall that, in single crystals, optical activity is a tensor property resulting from the spatial dispersion of the dielectric response, *i.e.* the breakdown of the usual electric dipole approximation in radiation–matter interactions. The interaction of an electromagnetic wave defined by a wavevector $|\mathbf{k}| = \omega/c$ with anisotropic media is usually described in terms of the dielectric permittivity tensor, which can be represented as the following sum (Agranovich & Ginzburg, 1984),

$$\varepsilon_{\alpha\beta}(\omega, \mathbf{k}) = \varepsilon_{\alpha\beta}(\omega) + ik_\eta \gamma_{\alpha\beta\eta}(\omega) + \alpha_{\alpha\beta\eta\delta}(\omega) k_\eta k_\delta + \ldots . \quad (1)$$

In absorbing media the components of each tensor in (1) are complex values, whose real and imaginary parts describe refraction and absorption processes, respectively.

Using Fermi's golden rule for the transition rate, the X-ray absorption cross section in Gaussian units is

$$\sigma = 4\pi^2 \alpha \frac{\hbar}{m^2 \omega} \sum_{i,f} \left| \langle f | \mathbf{p} \cdot \boldsymbol{\varepsilon} \exp(i\mathbf{k} \cdot \mathbf{r}) | i \rangle \right|^2 \delta(E_f - E_i - \hbar\omega), \quad (2)$$

where $\hbar\omega$ is the energy of the X-ray photon with unit polarization vector $\boldsymbol{\varepsilon}$. Labels *i* and *f* stand for initial (core) and final (empty) states with energies E_i and E_f. The conventional approach is to expand the exponent in equation (2) in powers of (**kr**),

$$\exp(i\mathbf{k} \cdot \mathbf{r}) \simeq 1 + i\mathbf{kr} + \frac{(i\mathbf{kr})^2}{2!} + \ldots . \quad (3)$$

The traditional dipole approximation corresponds to setting $\exp(i\mathbf{k} \cdot \mathbf{r}) = 1$; then the transition operator reduces to the so-called velocity form of the electric dipole (*E*1) operator. The above expansion is closely related to the expansion in terms of electromagnetic multipoles designated generically as *EJ* and *MJ*, *J* being the multipolarity. The first-order term is related to a linear combination of electric-quadrupole (*E*2) and magnetic-dipoles (*M*1) multipoles. The term, quadratic in *k*, corresponds to electric-octupole (*E*3) and magnetic-quadrupole (*M*2) multipoles. The multipoles behave as tensors of increasing rank (*J*) and alternating parity given by $(-1)^J$ for electric moments and $(-1)^{J-1}$ for magnetic ones. The validity of this approach in X-ray spectroscopy was discussed by Brouder (1990) and it was shown that the first two terms are sufficient to describe the X-ray absorption spectra. The cross section, equation (2), is proportional to the square of the transition amplitude and can be represented as the following sum,

$$\sigma(\omega) = \sigma^{E1.E1}_{\alpha\beta}(\omega) + \sigma^{E1.E2}_{\alpha\beta\eta}(\omega, \mathbf{k}) + \sigma^{E1.M1}_{\alpha\beta\eta}(\omega, \mathbf{k}) + \sigma^{E2.E2}_{\alpha\beta\eta\delta}(\omega, \mathbf{k}^2) + \sigma^{E2.M1}_{\alpha\beta\eta\delta}(\omega, \mathbf{k}^2) + \sigma^{M1.M1}_{\alpha\beta\eta\delta}(\omega, \mathbf{k}^2). \quad (4)$$

Let us underline the tensorial character of each contribution, which provides various kinds of X-ray optical effects at photon energies close to an absorption edge. The first term is the rank-2 tensor due to pure electric dipole transitions. Its symmetric part describes the linear dichroism effect. In the presence of an external magnetic field or spontaneous magnetic order, this tensor has an antisymmetric part that is at the origin of the magnetic circular dichroism. Further terms in the symmetrical part that are quadratic in the magnetization describe the magnetic linear dichroism. There are three terms which are quadratic in **k**; the last two are very weak in the X-ray range and will not be discussed here. The pure electric quadrupolar transitions give rise to the rank-4 tensor and there has been ample experimental evidence of their importance in X-ray absorption spectroscopy with photon energy above 4 keV (Brouder, 1990). The symmetric part of this tensor is responsible for an optical anisotropy including cubic crystals as was observed in the visible (Pastrnak & Vedam, 1971) as well as in the X-ray range (Cabaret *et al.*, 2001). Whenever the medium is magnetic or placed in an external magnetic field, this rank-4 tensor has also an antisymmetric part which leads to observation of magnetic circular dichroism. We are most concerned in the present paper with the rank-3 tensors in equation (4) which are linear in the X-ray wavevector. In the absence of any external magnetic field or any spontaneous magnetic ordering in the system, these tensors are fully antisymmetric and describe effects related to natural optical

activity. Let us stress again that the elements of these tensors are associated with transition probabilities that mix multipoles of opposite parity (*E*1.*E*2: electric-dipole–electric-quadrupole; *E*1.*M*1: electric-dipole–magnetic-dipole), and, thus, can be non-zero only in non-centrosymmetric systems. The sum of these two tensors is closely related to the imaginary parts of the rank-3 tensor (γ) in equation (1) called the gyration tensor. When a crystal is odd not only with respect to space parity but also with respect to the time-reversal operator, the gyration tensor may still exhibit a symmetric part. It has been shown (Smolenskii *et al.*, 1975) that the real and imaginary parts of the gyration tensor can be associated with four distinct classes of optical effects depending on their time-reversal symmetry. These are listed in Table 1 and each caters for a unique experimental technique for investigating specific properties of the material. If the sign of the effect changes when light propagates in the forward and backward directions, the effect is called non-reciprocal. A typical example of non-reciprocal effects is Faraday rotation. As can be seen from Table 1, all non-reciprocal optical activity effects are associated with broken time-reversal symmetry.

It has been shown (Agranovich & Ginzburg, 1984) that the gyration tensor is antisymmetric in the exchange of the first two indices,

$$\gamma_{\alpha\beta\eta} = -\gamma_{\beta\alpha\eta}. \tag{5}$$

Thus, in Cartesian coordinates, at most nine components out of 27 could be independent. This makes it often preferable to substitute $\gamma_{\alpha\beta\eta}$ by its dual, rank-2, gyrotropy tensor $G_{\alpha\beta}$ defined as

$$G_{\alpha\beta} = \frac{1}{2}\,\delta_{\alpha\lambda\mu}\gamma_{\lambda\mu\beta}, \tag{6}$$

where $\delta_{\alpha\lambda\mu}$ is the Levi–Civita symbol, or permutation tensor (Nye, 1957).

The gyrotropy tensor has three irreducible representations with respect to the operations of the rotation group SO_3 (Jerphagnon & Chemla, 1976): a pseudo-scalar, a polar vector and a traceless symmetric rank-2 pseudo-tensor called a pseudo-deviator. A pseudo-scalar and a pseudo-tensor are rotational invariants but, unlike a true scalar or a true tensor, they have odd parity and therefore all their components invert the signs under spatial inversion. On the other hand, only pseudo-scalar terms survive in randomly oriented samples (molecules in solution or powder) while the vector part and pseudo-deviator could be detected only in systems with an orientational order. *A priori* the scalar part of the gyrotropy tensor could only be associated with the *E*1.*M*1 interference terms. This is because the involved transition moment tensors are of equal rank. As far as X-ray spectroscopy is concerned, magnetic dipole transitions (*M*1) are forbidden due to the radial orthogonality of the core and the valence states involved in transitions. Nevertheless, a very weak XNCD signal due to the *E*1.*M*1 contribution was detected at the Ni *K*-edge in α-$NiSO_4{\cdot}6H_2O$ (Rogalev *et al.*, 2008*b*). This observation may perhaps indicate that magnetic dipole transitions become allowed in multi-electron processes involving valence electrons and which are not subject to standard selection rules.

Table 1
Properties of the gyration tensor $\gamma_{\alpha\beta\eta}$ under space inversion (parity operator *P*) and time-reversal (*T*) operations and corresponding optical effects in crystals.

Tensor	Part of tensor	*P*	*T*	Optical effect
Re $\gamma_{\alpha\beta\eta}$	Symmetric	−	−	Non-reciprocal linear dichroism
Im $\gamma_{\alpha\beta\eta}$	Symmetric	−	−	Non-reciprocal birefringence
Re $\gamma_{\alpha\beta\eta}$	Antisymmetric	−	+	Circular birefringence (optical activity)
Im $\gamma_{\alpha\beta\eta}$	Antisymmetric	−	+	Natural circular dichroism

At the same order of (**kr**) development as *E*1.*M*1 there is an interference term between the electric dipole and the electric quadrupole transition operators (*E*1.*E*2). Since these are tensors of unequal rank, the result cannot be a pseudo-scalar and this term would not therefore contribute in random orientation. The *E*1.*E*2 interference terms appear to be responsible for the vector part of optical activity and to strongly contribute to the pseudo-deviator. One should bear in mind that only 13 crystal classes (622; 32; 422; 6; 3; 4; $\bar{4}2m$; $\bar{4}$; *mm*2; 222; 2; *m*; 1) admit the pseudo-deviator as a rotational invariant in SO_3, so exhibiting XNCD as a consequence of non-vanishing tensor $\sigma^{E1.E2}_{\alpha\beta\eta}(\omega, \mathbf{k})$. It might be worth emphasizing here that only nine out of these 13 groups are enantiomorphous and that chirality and optical activity are two distinct physical concepts which should never be confused.

XNCD is defined as the difference in absorption cross sections for right $[\sigma^+(\omega)]$ and left $[\sigma^-(\omega)]$ circularly polarized X-ray beams,

$$\Delta\sigma_{\rm XNCD}(\omega) = \sigma^+(\omega) - \sigma^-(\omega).$$

At the microscopic level the electric-dipole–electric-quadrupole interference term is

$$\sigma^{E1.E2}(\omega) = 2\pi^2\alpha\hbar\omega i \sum_f \left(\langle f|\boldsymbol{\varepsilon}\cdot\mathbf{r}|i\rangle^*\langle f|\boldsymbol{\varepsilon}\cdot\mathbf{r}\mathbf{k}\cdot\mathbf{r}|i\rangle - \text{c.c.}\right) \times \delta(E_{\rm f} - E_{\rm i} - \hbar\omega), \tag{7}$$

where c.c. stands for complex conjugate. If one chooses the η-axis to be the X-ray beam propagation direction (**kr** = $k_\eta r_\eta$), the XNCD cross section due to *E*1.*E*2 interference terms takes the form

$$\begin{aligned}\Delta\sigma_{\rm XNCD}(\omega) &\propto k_\eta \sum_f \left(\langle i|r_\alpha|f\rangle\langle f|r_\beta r_\eta|i\rangle - \langle i|r_\alpha r_\eta|f\rangle\langle f|r_\beta|i\rangle\right) \\ &\quad\times \delta\left(E_{\rm f} - E_{\rm g} - \hbar\omega\right) \\ &\simeq k_\eta\,{\rm Im}\left(\gamma_{\alpha\beta\eta}\right).\end{aligned} \tag{8}$$

XNCD is linked to the imaginary part $\gamma''_{\alpha\beta\eta}$ of the gyration tensor. For a deeper insight into the physical origin of this effect it is instructive to relate the XNCD cross section to some ground-state observable, *i.e.* to some effective operator. This is precisely the aim of the spectroscopic sum rules. In 1998, Natoli *et al.* (Natoli *et al.*, 1998; Brouder *et al.*, 1999) showed that the XNCD integral is proportional to the ground-state rank-2 effective operator that probes the mixing of

orbitals of different parity in final states. At the K or L_1-edges, the degree of mixing of p- and d-orbitals is directly measured. Carra *et al.* (Carra & Benoist, 2000; Carra *et al.*, 2003) were the first to realize and to prove that the effective operator of XNCD is the dyad product of two vectors: the time-reversal odd orbital angular momentum vector and an orbital anapole moment (Khriplovich & Pospelov, 1990) which is odd with respect to both parity and time-reversal.

Experimentally, XNCD has been observed in quite a large number of non-centrosymmetric crystals (Natoli *et al.*, 1998; Okutani *et al.*, 1999; Peacock & Stewart, 2001; Goulon *et al.*, 2003*a*,*b*) but it is still less widely used in comparison with its magnetic counterpart. This technique could gain renewed interest with the emergence of new molecular materials which are both chiral and magnetic (Sessoli *et al.*, 2015).

3. X-ray optical activity in langasite crystal

Langasite, which has the chemical formula $La_3Ga_5SiO_{14}$, is a piezoelectric crystal of the same crystal class as quartz and hence possessing similar acoustic and optical properties (Belokoneva & Belov, 1981; Mill *et al.*, 1982). The first lanthanum gallium silicate crystals were grown in Russia in the early 1980s (Mill & Pisarevsky, 2000). The structure of langasite crystal belongs to the trigonal system with point group 32 [space group $P321$ (No.150), $Z = 1$, lattice constants a = 8.1746 (6) Å, c = 5.1022 (4) Å (Maksimov *et al.*, 2005)], being isostructural to $Ca_3Ga_2Ge_4O_{14}$ (Mill *et al.*, 1982).

There are four different cationic sites in the structure with generic chemical formula $A_3BC_3D_2O_{14}$. The A site (the Wyckoff position 3*e* with local symmetry 2), coordinated by eight oxygen atoms, can be represented as a distorted dodecahedron with trigonal faces, known as twisted Thomson. The octahedral B site is coordinated by six oxygen atoms and has position 1*a* with symmetry 32. Both C and D sites represent tetrahedral sites coordinated by four oxygen atoms, whereby the size of the C tetrahedra (position 3*f*, symmetry 2) is slightly larger than the D tetrahedra (2*d* position with symmetry 3). The structure is layered: along the c axis, tetrahedral layers alternate with layers composed of octahedra and dodecahedra (Fig. 1).

In the $La_3Ga_5SiO_{14}$ crystal structure, La^{3+} ions occupy the A site, Ga^{3+} are located at the B (Ga1), C (Ga3) and half of the D (Ga2) sites, whereas Si^{4+} ions occupy another half of the D site (see Fig. 2).

The space group $P321$ is symmorphic and there are no forbidden resonant reflections. Sometimes the resonant contribution can be extracted from the weakly allowed reflections (Mukhamedzhanov *et al.*, 2007) due to the interference between two scattering channels. But in this case the site-selective resonant contribution to the atomic factor is significantly less than the non-resonant contribution, which makes the resonant X-ray scattering unsuitable for studying local anisotropy in the $P321$ group crystals. On the other hand, this space group is enantiomorphic; that is to say, there should exist two chiral atomic arrangements, left- and right-handed. Crystals belonging to the 32 point group admit both a pseudo-scalar and a pseudo-deviator as rotational invariants and therefore are compatible with the observation of circular dichroism in the visible as well as in the X-ray range. Contrary to diffraction experiments which are sensitive to the phase shift of the waves scattered by different atoms, in absorption geometry the imaginary part of gyration tensor $\gamma''_{\alpha\beta\eta}$ describing circular dichroism in a crystal is a sum over all absorbing atoms,

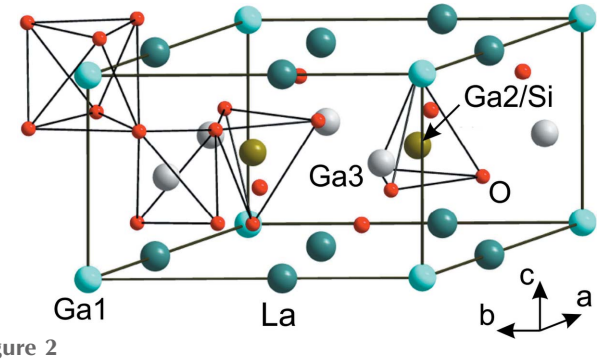

Figure 2
Crystal structure of $La_3Ga_5SiO_{14}$. Ga1 represents Ga ions in the octahedral 1*a* position, Ga2 corresponds to gallium ions in the tetrahedral 2*d* position and Ga3 denotes Ga in the 3*f* tetrahedral position.

$$\gamma''_{\alpha\beta\eta} = \sum_n \gamma''^{n}_{\alpha\beta\eta}, \tag{9}$$

where $\gamma''^{n}_{\alpha\beta\eta}$ is a third-rank tensor corresponding to the nth non-equivalent absorbing atom in a unit cell.

In general, this third-rank tensor antisymmetric in the exchange of the first two indices contains only nine independent non-zero components, which can be written in a matrix form as (Agranovich & Ginzburg, 1984; Sirotine & Shaskolskaia, 1982)

$$\gamma''_{\alpha\beta\eta} = \begin{pmatrix} \gamma''_{yzx} & \gamma''_{yzy} & \gamma''_{yzz} \\ \gamma''_{zxx} & \gamma''_{zxy} & \gamma''_{zxz} \\ \gamma''_{xyx} & \gamma''_{xyy} & \gamma''_{xyz} \end{pmatrix}. \tag{10}$$

In the $P321$ space group, atoms can occupy seven non-equivalent Wyckoff positions, 1*a*, 1*b*, 2*c*, 2*d*, 3*e*, 3*f* and 6*g* (Hahn, 2005). Positions 1*a* and 1*b* have site symmetry 32, positions 2*c* and 2*d* have site symmetry 3, positions 3*e* and 3*f* have site symmetry 2 and position 6*g* has site symmetry 1. Since atoms occupying Wyckoff positions with the same site symmetry have the same non-zero gyration tensor components, it is sufficient to calculate the gyration tensor for 1*a*, 2*d*, 3*f* and 6*g*.

There is only one atom with coordinates (0,0,0) and site symmetry 32 in position 1*a* of the $P321$ group, and its gyration tensor contains non-zero components (Sirotine & Shaskolskaia, 1982; Malgrange *et al.*, 2014),

$$\gamma''^{(1a)}_{\alpha\beta\eta} = \begin{pmatrix} \gamma''^{(1a)}_{yzx} & 0 & 0 \\ 0 & \gamma''^{(1a)}_{yzx} & 0 \\ 0 & 0 & \gamma''^{(1a)}_{xyz} \end{pmatrix}. \tag{11}$$

In position 3*f* there are three atoms with the coordinates $(x,0,1/2)$, $(0,x,1/2)$, $(-x,-x,1/2)$ whose site symmetry is 2. The

gyration tensor for each atom contains five non-zero components,

$$\gamma''^{(\mathrm{atom},3f)}_{\alpha\beta\eta} = \begin{pmatrix} \gamma''^{(3f)}_{yzx} & 0 & \gamma''^{(3f)}_{yzz} \\ 0 & \gamma''^{(3f)}_{zxy} & 0 \\ \gamma''^{(3f)}_{xyx} & 0 & \gamma''^{(3f)}_{xyz} \end{pmatrix}. \quad (12)$$

The tensor components of different atoms in position $3f$ are related by the threefold axis parallel to the c axis of the crystal. In the orthogonal basis, their coordinates are transformed as $\mathbf{r}' = T\mathbf{r}$, where T is the rotation matrix

$$T = \begin{pmatrix} -1/2 & -\sqrt{3}/2 & 0 \\ \sqrt{3}/2 & -1/2 & 0 \\ 0 & 0 & 1 \end{pmatrix}. \quad (13)$$

The gyration tensors for these atoms have the following forms,

$$\gamma''^{(A_1,3f)}_{\alpha\beta\eta} = \begin{pmatrix} \gamma''^{(3f)}_{yzx} & 0 & \gamma''^{(3f)}_{yzz} \\ 0 & \gamma''^{(3f)}_{zxy} & 0 \\ \gamma''^{(3f)}_{xyx} & 0 & \gamma''^{(3f)}_{xyz} \end{pmatrix},$$

$$\gamma''^{(A_2,3f)}_{\alpha\beta\eta} = \begin{pmatrix} \left(3\gamma''^{(3f)}_{zxy} + \gamma''^{(3f)}_{yzx}\right)/4 & \sqrt{3}\left(\gamma''^{(3f)}_{yzx} - \gamma''^{(3f)}_{yzz}\right)/4 & -\gamma''^{(3f)}_{yzz}/2 \\ \sqrt{3}\left(\gamma''^{(3f)}_{yzx} - \gamma''^{(3f)}_{yzz}\right)/4 & \left(\gamma''^{(3f)}_{zxy} + 3\gamma''^{(3f)}_{yzx}\right)/4 & -\sqrt{3}\gamma''^{(3f)}_{yzz}/2 \\ -\gamma''^{(3f)}_{yzz}/2 & -\sqrt{3}\gamma''^{(3f)}_{yzz}/2 & \gamma''^{(3f)}_{xyz} \end{pmatrix}, \quad (14)$$

$$\gamma''^{(A_3,3f)}_{\alpha\beta\eta} = \begin{pmatrix} \left(3\gamma''^{(3f)}_{zxy} + \gamma''^{(3f)}_{yzx}\right)/4 & -\sqrt{3}\left(\gamma''^{(3f)}_{yzx} - \gamma''^{(3f)}_{yzz}\right)/4 & -\gamma''^{(3f)}_{yzz}/2 \\ -\sqrt{3}\left(\gamma''^{(3f)}_{yzx} - \gamma''^{(3f)}_{yzz}\right)/4 & \left(\gamma''^{(3f)}_{zxy} + 3\gamma''^{(3f)}_{yzx}\right)/4 & \sqrt{3}\gamma''^{(3f)}_{yzz}/2 \\ -\gamma''^{(3f)}_{yzz}/2 & \sqrt{3}\gamma''^{(3f)}_{yzz}/2 & \gamma''^{(3f)}_{xyz} \end{pmatrix}.$$

The total gyration tensor corresponding to position $3f$ is the sum of the gyration tensors corresponding to each atom,

$$\gamma''^{(3f)}_{\alpha\beta\eta} = \gamma''^{(A_1,3f)}_{\alpha\beta\eta} + \gamma''^{(A_2,3f)}_{\alpha\beta\eta} + \gamma''^{(A_3,3f)}_{\alpha\beta\eta} = \begin{pmatrix} 3\left(\gamma''^{(3f)}_{zxy} + \gamma''^{(3f)}_{yzx}\right)/2 & 0 & 0 \\ 0 & 3\left(\gamma''^{(3f)}_{zxy} + \gamma''^{(3f)}_{yzx}\right)/2 & 0 \\ 0 & 0 & 3\gamma''^{(3f)}_{xyz} \end{pmatrix}. \quad (15)$$

There are two atoms in position $2d$ with site symmetry 3 which are connected by the twofold symmetry axis $[(1/3, 2/3, z) \rightarrow (2/3, 1/3, -z)]$. The gyration tensor for an atom in the $2d$ position is

$$\gamma''^{(\mathrm{atom},2d)}_{\alpha\beta\eta} = \begin{pmatrix} \gamma''^{(2d)}_{yzx} & \gamma''^{(2d)}_{yzy} & 0 \\ -\gamma''^{(2d)}_{yzy} & \gamma''^{(2d)}_{yzx} & 0 \\ 0 & 0 & \gamma''^{(2d)}_{xyz} \end{pmatrix}, \quad (16)$$

and the corresponding rotation matrix is given by

$$T = \begin{pmatrix} -1/2 & \sqrt{3}/2 & 0 \\ \sqrt{3}/2 & 1/2 & 0 \\ 0 & 0 & -1 \end{pmatrix}. \quad (17)$$

Hence, the resulting gyration tensor corresponding to position $2d$ is the sum of the gyration tensors corresponding to each atom,

$$\gamma''^{(2d)}_{\alpha\beta\eta} = \begin{pmatrix} 2\gamma''^{(2d)}_{yzx} & 0 & 0 \\ 0 & 2\gamma''^{(2d)}_{yzx} & 0 \\ 0 & 0 & 2\gamma''^{(2d)}_{xyz} \end{pmatrix}. \quad (18)$$

There are six atoms, (x,y,z), $(-y,x-y,z)$, $(-x+y,-x,z)$, $(y,x,-z)$, $(x-y,-y,z)$, $(-x,-x+y,z)$, with site symmetry 1 in position $6g$, and the gyration tensor for each atom contains non-zero components,

$$\gamma''^{(\mathrm{atom},6g)}_{\alpha\beta\eta} = \begin{pmatrix} \gamma''^{(6g)}_{yzx} & \gamma''^{(6g)}_{yzy} & \gamma''^{(6g)}_{yzz} \\ \gamma''^{(6g)}_{zxx} & \gamma''^{(6g)}_{zxy} & \gamma''^{(6g)}_{zxz} \\ \gamma''^{(6g)}_{xyx} & \gamma''^{(6g)}_{xyy} & \gamma''^{(6g)}_{xyz} \end{pmatrix}. \quad (19)$$

The resulting gyration tensor corresponding to position $6g$ is the sum of the gyration tensors corresponding to each atom,

$$\gamma''^{(6g)}_{\alpha\beta\eta} = \begin{pmatrix} 3\left(\gamma''^{(6g)}_{yzx} + \gamma''^{(6g)}_{zxy}\right) & 0 & 0 \\ 0 & 3\left(\gamma''^{(6g)}_{yzx} + \gamma''^{(6g)}_{zxy}\right) & 0 \\ 0 & 0 & 6\gamma''^{(6g)}_{xyz} \end{pmatrix}. \quad (20)$$

Thus, circular dichroism in a crystal with $P321$ space group can be completely described by combining tensors (11), (15), (18) and (20). For example, Ga^{3+} ions in $La_3Ga_5SiO_{14}$ crystal occupy three Wyckoff positions, $1a$, $3f$ and $2d$ (the latter in a ratio of 1:1 with Si^{4+} ions). The resulting gyration tensor for Ga atoms is the sum of the gyration tensors corresponding to Ga atoms in each position,

$$\gamma''_{\alpha\beta\eta} = \gamma''^{(1a)}_{\alpha\beta\eta} + \frac{1}{2}\gamma''^{(2d)}_{\alpha\beta\eta} + \gamma''^{(3f)}_{\alpha\beta\eta} = \begin{pmatrix} \gamma''_{yzx} & 0 & 0 \\ 0 & \gamma''_{yzx} & 0 \\ 0 & 0 & \gamma''_{xyz} \end{pmatrix}, \quad (21)$$

where

$$\gamma''_{yzx} = \gamma''^{(1a)}_{yzx} + \gamma''^{(2d)}_{yzx} + 3\left(\gamma''^{(3f)}_{yzx} + \gamma''^{(3f)}_{zxy}\right)/2$$

and

$$\gamma''_{xyz} = \gamma''^{(1a)}_{xyz} + \gamma''^{(2d)}_{xyz} + 3\gamma''^{(3f)}_{xyz}.$$

Note that due to the symmetry of the $2d$ and $3f$ positions the tensor components $\gamma''^{(2d)}_{yzy}$, $\gamma''^{(3f)}_{xyx}$ and $\gamma''^{(3f)}_{yzz}$ do not contribute to the tensor γ''.

If one chooses the z-axis (optical axis of the crystal) collinear with the X-ray wavevector ($\mathbf{kr} = \underline{kz}$), the XNCD cross section (8) due to $E1.E2$ transitions is given by

$$\Delta\sigma^{\parallel}_{\mathrm{XNCD}}(\omega) = 4\pi^2\alpha\hbar\omega k_z \times \sum_c \left(\langle a|x|c\rangle\langle c|yz|a\rangle - \langle a|zx|c\rangle\langle c|y|a\rangle\right) \simeq k_z\gamma''_{xyz}, \quad (22)$$

whereas, for the X-ray beam directed along the x-axis (and similarly along the y-axis),

$$\Delta\sigma^{\perp}_{\mathrm{XNCD}}(\omega) = 4\pi^2\alpha\hbar\omega k_x \times \sum_c \left(\langle a|y|c\rangle\langle c|xz|a\rangle - \langle a|yx|c\rangle\langle c|z|a\rangle\right) \simeq k_x\gamma''_{yzx}. \quad (23)$$

Here, we have neglected the pseudo-scalar $E1.M1$ contributions, which is a well justified approximation for the X-ray range and that imposes an additional symmetry restriction of the components of the gyration tensor, *i.e.* $\gamma''_{yzx} + \gamma''_{yzx} + \gamma''_{xyz} = 0$ or $\gamma''_{xyz} = -2\gamma''_{yzx}$. This is manifested in the angular dependence of XNCD spectra for uniaxial crystals being proportional to $3\cos^2\theta - 1$ (Natoli *et al.*, 1998), where θ is an angle between the X-ray propagation direction and the optical axis of the crystal.

4. Experiment

A high-quality single crystal of $La_3Ga_5SiO_{14}$ was grown by the Czochralski method at M. V. Lomonosov Moscow State University. For the experiment described in this paper the sample was cut in the form of a 5 mm × 5 mm × 2 mm parallelepiped with the *c*-axis perpendicular to a large surface. It was optically polished and checked to be enantiopure. The XNCD spectra were recorded at ESRF beamline ID12 dedicated to polarization-dependent X-ray spectroscopy in the X-ray range from 2 to 15 keV. The performances of this beamline are described by Rogalev *et al.* (2001) and we are limiting ourselves here only to details relevant to the present experiment. The source of circularly polarized X-rays is the helical undulator of APPLE-II type, the fundamental harmonic of which covers the energy range 5.0–8.9 keV. For the experiments at the *K*-edge of Ga (∼10.37 keV), we had to use the second harmonic of the undulator emission. The X-ray beam has been further monochromated using a fixed-exit double-crystal monochromator equipped with a pair of Si(111) crystals cooled down to 133 K. Given the very low emittance of the electron beam at the ESRF, the instrumental energy resolution at the Ga *K*-edge of 1.5 eV is better than the natural width (FWHM: full width at half maximum) of the 1*s* core level, ∼1.8 eV (Krause & Oliver, 1979).

The dichroic signal is proportional to the circular polarization rate of the monochromatic X-ray beam which is defined as the ratio of the difference between the intensity I_R and I_L of the right- and left-handed circularly polarized beams to the sum of these intensities, $(I_R - I_L)/(I_R + I_L)$. X-ray polarimetry analyses have shown that, at the Ga *K*-edge and under the present experimental conditions, it exceeds 0.95. X-ray absorption spectra were recorded at room temperature using total X-ray fluorescence yield detection mode. Due to the known saturation and self-absorption effects, the fluorescence signal is not linearly related to the X-ray absorption spectrum (Goulon *et al.*, 1982). There is a fairly simple transformation of fluorescence data, which is generally used to reconstruct the absorption coefficient (Loos *et al.*, 1989). The XNCD spectra were obtained as the direct difference of two X-ray absorption spectra recorded with right- and left-circularly polarized X-rays. The XNCD spectra have been recorded for two experimental configurations: (*a*) the X-ray wavevector of incident radiation is parallel to the crystal *c*-axis ($\Delta\sigma^{\parallel}_{XNCD}$) and (*b*) the wavevector is parallel to the *a*-axis ($\Delta\sigma^{\perp}_{XNCD}$).

5. Results and discussion

The study of langasite electronic structure by optical methods (Kitaura *et al.*, 2004) has shown that the valence band is mainly formed by the O 2*p* states, the lower part of the conduction band is dominated by the La 5*d* states, while the upper part is built up of the Ga 4*p* states with small hybridization with the Si 3*s* and 3*p* states. There is no optical data about *p*–*d* or *d*–*f* hybridization. In contrast to the visible range, OA in the X-ray range is observed near resonant transitions between an inner atomic shell and an excited state of the outer electron shells, which are subjected to the action of the crystal field and interatomic interactions. In the case of the *K*-edge of Ga, for example, XNCD spectra will probe the on-site hybridization of *p*- and *d*-states. As in optics, the outer states can be localized or delocalized. There have been some discussions about the degree of localization of excited electronic states giving the main contribution to the visible OA in langasite (Burkov *et al.*, 2008; Qi *et al.*, 2005; Veremeichik, 2011). X-ray spectroscopy could shed some light on this, since excitations to localized states give a contribution to the X-ray absorption spectrum predominantly in the pre-edge region, whereas transitions to delocalized states contribute at photon energies above the absorption edge. So, the measurement of the XNCD signal in langasite will give additional information about its electronic structure, which could be further used for understanding the unusual optical properties of this family of crystals.

The experiment has shown the existence of the XNCD spectra at the *K*-edge of Ga mainly above the edge with a minor contribution at the pre-edge (see Fig. 3). The XNCD spectra were found to be twice as large for experiments with the wavevector along the *c*-axis and to have the opposite sign for measurements for the wavevector perpendicular to the *c*-axis, as expected from the angular dependence of XNCD for uniaxial crystals, $\sim 3\cos^2\theta - 1$ (Natoli *et al.*, 1998), and as follows from the symmetry consideration (here θ is the angle

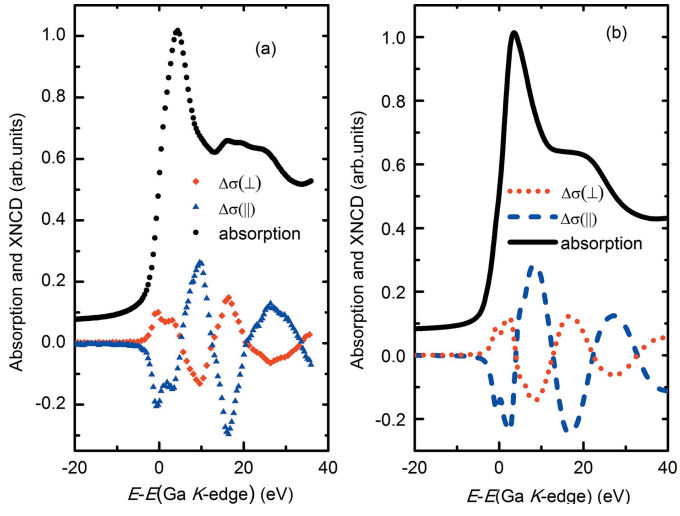

Figure 3
Absorption (dots) and XNCD [$\Delta\sigma(\perp) = \Delta\sigma^{\perp}_{XNCD}$ $\Delta\sigma^{\perp}_{XNCD}$ × 50, $\Delta\sigma(\parallel) = \Delta\sigma^{\parallel}_{XNCD}$ × 50] spectra of langasite crystal near the Ga *K*-edge: experiment (*a*) *versus* calculation (*b*). *E*(Ga *K*-edge) = 10367 eV.

between the **k** vector and the *c*-axis). Up to now the XNCD was measured mainly in the structures whose chirality was determined by a screw axis (Goulon *et al.*, 1998; Alagna *et al.*, 1998; Rogalev *et al.*, 2008*a*). In the majority of cases, the XNCD signal has an extended spectral shape above the edge, but sometimes it is localized in the pre-edge (Rogalev *et al.*, 2008*a*). It is clear that there are two factors determining the energy dependence and the shape of the XNCD signal: the density of states and local chiral environment of the absorbing atom.

The experimentally observed absorption and XNCD signal at the Ga *K*-edge are the sum of the contributions corresponding to each non-equivalent position and are proportional to the sum of the third-rank tensor components describing each absorbing Ga atom [see equation (21)]. There is no way to separate the XNCD signals from various positions experimentally neither in the visible nor in the X-ray range. Nevertheless, it is interesting to know the XNCD signal corresponding to three different Ga positions, because it reflects the unoccupied density of states of hybridized orbitals at each specific Wyckoff position. To disentangle the contributions from different Ga positions, we have performed *ab initio* calculations of XNCD spectra using the *FDMNES* code (Bunău & Joly, 2012). Computations performed with the *FDMNES* program allow us to calculate all the tensor components $\gamma''^{(s)}_{\alpha\beta\eta}$ for Ga atoms in each position. We restrict ourselves to only those components $\gamma''^{(s)}_{\alpha\beta\eta}$ that contribute to the XNCD signal and the sum of which can be directly compared with experimental results.

We have simultaneously simulated the Ga *K*-edge absorption and XNCD spectra and compared them with the experimental results. Calculations were performed for langasite structure parameters from Maksimov *et al.* (2005). The calculations were made using the multiple-scattering model with 195 atoms inside a sphere of radius 8.6 Å, as a further increase of the sphere size did not lead to any improvement. The spectra were convolved with a Lorentzian with an energy-dependent width, to take into account the core-hole lifetime assuming it to be the same for all Ga positions. A rather good overall agreement is obtained between calculated and experimental absorption and XNCD spectra, as illustrated in Figs. 3(*a*) and 3(*b*).

To compare the cross density of mixed states and to obtain the tensor components $\gamma_{\alpha\beta\eta}$ corresponding to each Ga position it is reasonable to calculate the XNCD per atom in each position. Certainly the largest contribution to the absorption and to the XNCD signal is expected from the 3*f* position which contains three times more Ga atoms compared with the 1*a* and 2*d* positions. The absorption and XNCD per Ga atom in three different crystallographic positions are shown in Figs. 4(*a*) and 4(*b*). The spectra corresponding to each Ga position are shifted along the vertical axis for clarity. The spectral shape of absorption and XNCD signals corresponding to each Ga position are different. This is not surprising taking into account the difference of their local environment.

The free ions La^{3+} and Si^{4+} have the electron shells ns^2np^6 of the noble gas type ^1S; the outer 3*d* shell of Ga^{3+} is expected

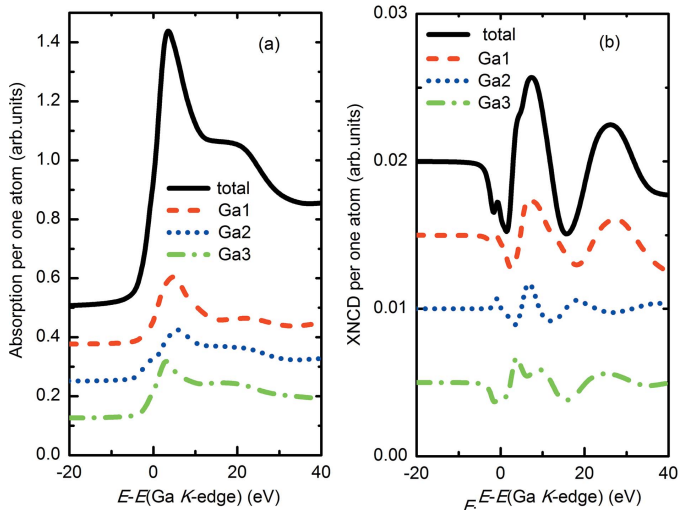

Figure 4
(*a*) Calculated absorption spectra of Ga in langasite crystal (total) and partial absorption spectra corresponding to Ga1, Ga2 and Ga3 positions per atom near the Ga *K*-edge. (*b*) Calculated XNCD spectra ($\Delta\sigma^{\parallel}_{\rm XNCD} = \gamma''_{xyz}$) of langasite crystal (total) and tensor components γ''_{xyz} spectra corresponding to Ga1 ($\gamma''^{(1a)}_{xyz}$), Ga2 ($\gamma''^{(2d)}_{xyz}$) and Ga3 ($\gamma''^{(3f)}_{xyz}$) positions near the Ga *K*-edge.

to be filled. In the visible region, the OA of langasite is very sensitive to the size of the structural polyhedra; first and foremost, the 3*e* oxygen dodecahedron and 1*a* Ga octahedron (Burkov *et al.*, 2008; Qi *et al.*, 2005; Veremeichik, 2011; Kitaura *et al.*, 2004). In the X-ray region, the shapes of the polyhedra are also essential because they influence the splitting of the electronic levels of absorbing atoms and in the multiple scattering model are described by different scattering paths. Usually the pre-edge peaks in *K*-edge XANES spectra are due to transitions into localized *d*-states (quadrupole peaks). Because of the absence of the pre-edge features in both XANES and in XNCD spectra we conclude that *d*- or *p*–*d*-hybridized electronic states of Ga are delocalized in langasite (see Fig. 3). This conclusion confirms the delocalization of chemical bonds deduced from experiments in the visible spectral range (Burkov *et al.*, 2008; Qi *et al.*, 2005; Veremeichik, 2011; Kitaura *et al.*, 2004). This result is in fact an expected one, since 3*d*-states of Ga are fully occupied and quadrupolar transitions are to empty 4*d*-states.

Figs. 4(*a*) and 4(*b*) show the partial absorption and XNCD spectra and tensor components corresponding to Ga atoms in three non-equivalent crystallographic positions. We can see that in the absorption spectra the strongest 'white line' corresponds to Ga in the 1*a* position. Usually the white line is proportional to the number of holes in the valence band with a symmetry defined by the selection rules for optical transitions, *e.g.* 4*p* holes at the *K*-edge of Ga. The 1*a* position possesses the highest symmetry 32 (distorted octahedra), maximal volume of surrounding oxygen polyhedra (interatomic distance Ga1–O 1.99 Å) and maximal distance for the six next-neighboring Ga (3.197 Å). Ga2 atoms in the 2*d* position are inside the distorted tetrahedra (1.795–1.805 Å) and three next-neighboring Ga at 3.221 Å. Ga3 3*f* atoms are inside the distorted tetrahedra formed by O atoms in the first sphere (1.805–

1.897 Å), two O atoms at 2.653 Å and six Ga atoms between 3.198 Å and 3.33 Å. In all cases the asymmetry of the environment (without inversion center) provides the splitting of electronic *p*- and *d*-states. The strength of the white line can be explained by different charges of ions corresponding to each Ga position. Calculations give the ion charges: 3.401 for the 1*a* position, 3.389 for the 2*d* position and 3.397 for the 3*f* position. So, the number of holes is maximal for the 1*a* position, followed by the strongest white line in the absorption spectrum.

As described above, Fig. 4(*b*) shows the calculated tensor components $\gamma''^{(s)}_{xyz}$ for Ga in each position. We can also see from Fig. 4(*b*) that spectral shapes are different reflecting the dependence on the local environment of the absorbing atom. These results could be correlated with an interesting explanation of the chiral properties of $Nd_3Ga_5SiO_{14}$ (langasite family) that was given by Dudka & Mill (2013, 2014). The electron density fragments forming helixes along the *c*-axis together with splitting of atomic environments due to statistical occupation of the 2*d* position were suggested as a structural basis for the chirality of langasites. It could be expected that similar pseudohelices would exist in the other langasite compounds providing multiferroism in the presence of magnetic ordering. This emphasizes the importance of further detailed studies of local chiral atomic arrangements in the langasite family of crystals.

6. Conclusion

Natural circular dichroism of langasite $La_3Ga_5SiO_{14}$ single crystal was studied experimentally and theoretically at the Ga *K*-edge. The XMCD spectrum measured along the *c*-axis of the crystal was found to be twice as strong as that recorded perpendicularly to it and has the opposite sign. This is in perfect agreement with the crystal structure and confirms the high quality of the crystal studied. The XNCD spectra have a spectral shape extended above the absorption edge without a strong feature in the pre-edge. Thus the hybridized *p*–*d* electronic states of Ga are mainly delocalized.

Microscopic and macroscopic approaches to the description of X-ray optical activity are discussed in detail. The macroscopic approach is formulated in terms of the gyration tensor. Consideration of the symmetry properties of the gyration tensor or gyrotropy tensor allows us to determine those tensor components that are responsible for the optical activity. The microscopic approach is based on multipole expansion of the transition operator. The antisymmetric part of the $\sigma^{E1.E2}$ tensor is responsible for X-ray natural circular dichroism, contrary to the visible optics where the *E*1.*M*1 pseudo-scalar term prevails. In the X-ray region, we deal with microscopic tensors describing the properties of absorbing atoms, which depend on the symmetry of the atomic sites. For each atomic site, a third-rank gyration tensor is invariant under the symmetry operation of a point group characteristic of a given Wyckoff position. The tensor $\gamma_{\alpha\beta\eta}$ describing XNCD of a crystal is the sum over all absorbing atoms in the unit cell. The gyration tensors for each Wyckoff position of the *P*321 space group occupied by Ga atoms have been explicitly given.

It was shown that the symmetry of $La_3Ga_5SiO_{14}$ allows two antisymmetric third-rank tensor components $\gamma''_{yzx} = \gamma''_{zxy}$ and $\gamma''_{xyz} = -2\gamma''_{yzx}$, which provide XNCD signal with the wavevector perpendicular and along the threefold symmetry axis. Both components are the sum over three atomic positions (1*a*, 2*d* and 3*f*). Because the space group of langasite does not provide any forbidden reflections, X-ray resonant diffraction cannot be exploited to obtain the site-selective information. So, there is no possibility of separating each contribution to the XNCD signal exclusively from experiment.

To obtain site-selective information, *ab initio* calculations of the absorption and XNCD spectra were carried out in the present study. A comparison of the results of calculations with the experimental data confirms their reliability and allows us to extract energy spectra corresponding to each of three non-equivalent Ga positions. The difference between the spectra corresponding to each of the Ga sites clearly reveals the different density of the *p*–*d* mixed electronic states of Ga in the 1*a*, 2*d* and 3*f* positions. Calculations have also shown that the strongest contribution to XNCD at the Ga *K*-edge arises from Ga in the 1*a* position. Finally, the combination of *ab initio* calculations with high-quality experimental results is shown to be a very valuable approach to studying the local chirality in multicomponent crystals like langasite.

Acknowledgements

The research was carried out using the equipment of the shared research facilities of HPC computing resources at Lomonosov Moscow State University.

Funding information

The following funding is acknowledged: Russian Foundation for Basic Research (grant No. 16-02-00887). The work of VED was supported by the grant 'NANO' of the Presidium of Russian Academy of Sciences.

References

Adachi, M., Funakawa, T. & Karaki, T. (2003). *Ferroelectrics*, **286**, 43–48.
Agranovich, V. M. & Ginzburg, V. L. (1984). *Spatial Dispersion in Crystal Optics and Theory of Excitons.* Berlin: Springer.
Alagna, L., Prosperi, T., Turchini, S., Goulon, J., Rogalev, A., Goulon-Ginet, C., Natoli, C. R., Peacock, R. D. & Stewart, B. (1998). *Phys. Rev. Lett.* **80**, 4799–4802.
Arago, D.-F.-M. (1811). *Mem. Inst. Fr. (Paris)*, **12**, 93–134.
Barron, L. D. (1971). *Mol. Phys.* **21**, 241–246.
Barron, L. D. (1982). *Molecular Light Scattering and Optical Activity*. Cambridge University Press.
Belokoneva, E. L. & Belov, N. V. (1981). *Dokl. Akad. Nauk SSSR*, **260**, 1363–1366.
Biot, J.-B. (1812). *Mem. Inst. Fr. (Paris)*, **13**, 218–253.
Brouder, Ch. (1990). *J. Phys. Condens. Matter*, **2**, 701–738.
Brouder, Ch., Juhin, A., Bordage, A. & Arrio, M.-A. (2008). *J. Phys. Condens. Matter*, **20**, 4552205.
Brouder, C., Natoli, C. R., Sainctavit, P., Goulon, J., Goulon-Ginet, C. & Rogalev, A. (1999). *J. Synchrotron Rad.* **6**, 261–263.

Buckingham, A. D. & Dunne, M. B. (1971). *J. Chem. Soc. A*, pp. 1988–1991.

Bunău, O. & Joly, Y. (2012). *Phys. Rev. B*, **85**, 155121.

Burkov, V. I., Perederei, E. P., Fedotov, E. V., Mill, B. V. & Pisarevskii, Yu. V. (2008). *Crystallogr. Rep.* **53**, 843–846.

Cabaret, D., Brouder, C., Arrio, M.-A., Sainctavit, P., Joly, Y., Rogalev, A. & Goulon, J. (2001). *J. Synchrotron Rad.* **8**, 460–462.

Carra, P. & Benoist, R. (2000). *Phys. Rev. B*, **62**, R7703–R7706.

Carra, P., Jerez, A. & Marri, I. (2003). *Phys. Rev. B*, **67**, 045111.

Chilla, E., Flannery, C. M., Fröhlich, H.-J. & Straube, U. (2001). *J. Appl. Phys.* **90**, 6084–6091.

Cotton, A. (1895). *CR Acad. Sci. (Paris)*, **120**, 989–1044.

Dmitrienko, V. E., Ishida, K., Kirfel, A. & Ovchinnikova, E. N. (2005). *Acta Cryst.* A**61**, 481–493.

Dudka, A. P. & Mill, B. V. (2013). *Crystallogr. Rep.* **58**, 593–602.

Dudka, A. P. & Mill, B. V. (2014). *Crystallogr. Rep.* **59**, 689–698.

Goulon, J., Goulon-Ginet, C., Cortes, R. & Dubois, J. M. (1982). *J. Phys. Fr.* **43**, 539–548.

Goulon, J., Goulon-Ginet, C., Rogalev, A., Gotte, V., Malgrange, C. & Brouder, C. (1999). *J. Synchrotron Rad.* **6**, 673–675.

Goulon, J., Goulon-Ginet, C., Rogalev, A., Gotte, V., Malgrange, C., Brouder, Ch. & Natoli, C. R. (1998). *J. Chem. Phys.* **108**, 6394–6403.

Goulon, J., Jaouen, N., Rogalev, A., Wilhelm, F., Goulon-Ginet, C., Brouder, Ch., Joly, Y., Ovchinnikova, E. N. & Dmitrienko, V. E. (2007). *J. Phys. Condens. Matter*, **19**, 156201.

Goulon, J., Rogalev, A., Goulon-Ginet, C., Benayoun, G., Paolasini, L., Brouder, C., Malgrange, C. & Metcalf, A. (2000). *Phys. Rev. Lett.* **85**, 4385–4388.

Goulon, J., Rogalev, A., Wilhelm, F., Goulon-Ginet, C., Carra, P., Cabaret, D. & Brouder, Ch. (2002). *Phys. Rev. Lett.* **88**, 237401.

Goulon, J., Rogalev, A., Wilhelm, F., Goulon-Ginet, C., Carra, P., Marri, I. & Brouder, Ch. (2003*a*). *J. Exp. Theor. Phys.* **97**, 402–431.

Goulon, J., Rogalev, A., Wilhelm, F., Jaouen, N., Goulon-Ginet, C. & Brouder, Ch. (2003*b*). *J. Phys. Condens. Matter*, **15**, S633–S645.

Hahn, T. (2005). *International Tables for Crystallography*, Vol. A, *Space-Group Symmetry*, 5th ed. Dordrecht: Springer.

Hodeau, J.-L., Favre-Nicolin, V., Bos, S., Renevier, H., Lorenzo, E. & Berar, J.-F. (2001). *Chem. Rev.* **101**, 1843–1867.

Jerphagnon, J. & Chemla, D. S. (1976). *J. Chem. Phys.* **65**, 1522–1529.

Jerphagnon, J., Chemla, D. S. & Bonneville, R. (1978). *Adv. Phys.* **27**, 609–650.

Khriplovich, I. B. & Pospelov, M. E. (1990). *Z. Phys. D*, **17**, 81–84.

Kitaura, M., Mochizuki, K., Inabe, Y., Itoh, M., Nakagawa, H. & Oishi, S. (2004). *Phys. Rev. B*, **69**, 115120.

Krause, M. & Oliver, J. (1979). *J. Phys. Chem. Ref. Data*, **8**, 329–338.

Laan, G. van der (2001). *J. Synchrotron Rad.* **8**, 1059–1060.

Landau, L. D. & Lifshitz, E. M. (1960). *Electrodynamics of Continuous Media.* Oxford: Pergamon Press.

Lee, C., Kan, E., Xiang, H. & Whangbo, M. H. (2010). *Chem. Mater.* **22**, 5290–5295.

Loos, M., Ascone, I., Goulon-Ginet, C., Goulon, J., Guillard, C., Lacroix, M., Breysse, M., Faure, D. & Descourieres, T. (1989). *Physica B*, **158**, 145–148.

Maksimov, B. A., Molchanov, V. N., Mill, B. V., Belokoneva, E. L., Rabadanov, M. Kh., Pugacheva, A. A., Pisarevskii, Yu. V. & Simonov, V. I. (2005). *Crystallogr. Rep.* **50**, 751–758.

Malgrange, C., Ricolleau, Ch. & Schlenker, M. (2014). *Symmetry and Physical Properties of Crystals.* Berlin: Springer.

Marty, K., Bordet, P., Simonet, V., Loire, M., Ballou, R., Darie, C., Kljun, J., Bonville, P., Isnard, O., Lejay, P., Zawilski, B. & Simon, Ch. (2010). *Phys. Rev. B*, **81**, 054416.

Mill, B. V., Butashin, A. V., Khodzhabagyan, G. G., Belokoneva, E. L. & Belov, N. V. (1982). *Dokl. Akad. Nauk SSSR*, **264**, 1385–1389.

Mill, B. V. & Pisarevsky, Y. V. (2000). *Proceedings of the 2000 IEEE/EIA International Frequency Control Symposium and Exhibition*, 9 June 2000, Kansas City, MO, USA, pp. 133–144.

Mukhamedzhanov, E. Kh., Borisov, M. M., Morkovin, A. N., Antonenko, A. A., Oreshko, A. P., Ovchinnikova, E. N. & Dmitrienko, V. E. (2007). *JETP Lett.* **86**, 783–787.

Natoli, C. R., Brouder, Ch., Sainctavit, Ph., Goulon, J., Goulon-Ginet, C. & Rogalev, A. (1998). *Eur. Phys. J. B*, **4**, 1–11.

Nye, J. F. (1957). *Physical Properties of Crystals.* Oxford University Press.

Ohsato, H., Iwataki, T. & Morikoshi, H. (2012). *Trans. Electr. Electron. Mater.* **13**, 171–176.

Okutani, M., Jo, T. & Carra, P. (1999). *J. Phys. Soc. Jpn*, **68**, 3191–3194.

Pastrnak, J. & Vedam, K. (1971). *Phys. Rev. B*, **3**, 2567–2571.

Peacock, R. D. & Stewart, B. (2001). *J. Phys. Chem. B*, **105**, 351–360.

Pikin, S. A. & Lyubutin, I. S. (2012). *Phys. Rev. B*, **86**, 064414.

Qi, H., Wei, A. & Yuan, D. (2005). *Mater. Sci. Eng. B*, **117**, 143–145.

Ramakrishnan, M., Joly, Y., Windsor, Y. W., Rettig, L., Alberca, A., Bothschafter, E. M., Lejay, P., Ballou, R., Simonet, V., Scagnoli, V. & Staub, U. (2017). *Phys. Rev. B*, **95**, 205145.

Rogalev, A., Goulon, J., Goulon-Ginet, C. & Malgrange, C. (2001). *Springer Lecture Notes in Physics*, Vol. 565, pp. 60–86. Berlin: Springer.

Rogalev, A., Goulon, J., Wilhelm, F. & Bosak, A. (2008*b*). *Springer Proceedings in Physics*, Vol. 133, pp. 169–190. Berlin/Heidelberg: Springer.

Rogalev, A., Goulon, J., Wilhelm, F., Kozlovskaya, K. A., Ovchinnikova, E. N., Soboleva, L. V., Konstantinova, A. F. & Dmitrienko, V. E. (2008*a*). *Crystallogr. Rep.* **53**, 384–390.

Röntgen, W. C. (1898). *Ann. Phys.* **300**, 12–17.

Roshchupkin, D. V., Irzhak, D. V., Tucoulou, R. & Buzanov, O. A. (2003). *J. Appl. Phys.* **94**, 6692–6696.

Sato, J., Takeda, H., Morikoshi, H., Shimamura, K., Rudolph, P. & Fukuda, T. (1998). *J. Cryst. Growth*, **191**, 746–753.

Scagnoli, V., Huang, S. W., Garganourakis, M., de Souza, R. A., Staub, U., Simonet, V., Lejay, P. & Ballou, R. (2013). *Phys. Rev. B*, **88**, 104417.

Sessoli, R., Boulon, M.-E., Caneschi, A., Mannini, M., Poggini, L., Wilhelm, F. & Rogalev, A. (2015). *Nat. Phys.* **11**, 69–74.

Sirotine, Yu. & Shaskolskaia, M. P. (1982). *Fundamentals of Crystal Physics.* Moscow: Mir.

Smolenskii, G. A., Pisarev, R. V. & Sinii, I. G. (1975). *Sov. Phys. Usp.* **18**, 410–429.

Stade, J., Bohatý, L., Hengst, M. & Heimann, R. B. (2002). *Cryst. Res. Technol.* **37**, 1113–1120.

Stewart, B., Peacock, R. D., Alagna, L., Prosperi, T., Turchini, S., Goulon, J., Rogalev, A. & Goulon-Ginet, C. (1999). *J. Am. Chem. Soc.* **121**, 10233–10234.

Takeda, H., Yamaura, J., Hoshina, T. & Tsusrumi, T. (2011). *Mater. Sci. Eng.* **18**, 092020.

Veremeichik, T. F. (2011). *Crystallogr. Rep.* **56**, 1060–1065.

Yariv, A. & Yeh, P. (1984). *Optical Waves in Crystals.* New York: Wiley.

Zorko, A., Pregelj, M., Potočnik, A., van Tol, J., Ozarowski, A., Simonet, V., Lejay, P., Petit, S. & Ballou, R. (2011). *Phys. Rev. Lett.* **107**, 257203.